Available online at www.sciencedirect.com
ScienceDirect
Journal of Sound and Vibration 297 (2006) 880–894
JOURNAL OF SOUND AND VIBRATION
www.elsevier.com/locate/jsvi

Modal analysis of cantilever plates undergoing accelerated in-plane motion

Hong Seok Lim, Hong Hee Yoo*

School of Mechanical Engineering, Hanyang University, 17 Haengdang-Dong Sungdong-Gu, Seoul 133-791, South Korea

Received 20 July 2005; received in revised form 19 April 2006; accepted 2 May 2006
Available online 30 June 2006

Abstract

A modeling method for the modal analysis of cantilever plates undergoing accelerated in-plane motion is presented in this paper. Von Karman strain measures are employed to derive the in-plane and the lateral equations of motion. In-plane strain measures of the accelerated plates are obtained from the in-plane equations and substituted into the lateral equations to obtain the linear equations for modal analysis. The resulting equations are transformed into dimensionless forms in which dimensionless parameters are identified. The effects of dimensionless parameter variations on the modal characteristics of the accelerated plates are investigated through numerical studies.
© 2006 Elsevier Ltd. All rights reserved.

1. Introduction

Flexible cantilever plate-like structures undergoing translational rigid body motion can be found in practical engineering examples such as aircraft wings and rocket fins. For the design of these structures, their modal characteristics are frequently obtained under the assumptions that the structures are stationary. Even if the structures undergo translational motions with constant velocity, their modal characteristics remain the same as those of the stationary structures. However, the structures often undergo accelerated motions that could result in significant variations of their modal characteristics. For instance, when an aircraft or a rocket takes off, their wings or fins undergo accelerated motion. Such an accelerated motion induces in-plane strains (due to inertia force) for the plate-like structures that effectively cause the variations of their modal characteristics. Since the take-off stage is critically important for the successful flight of the aircraft or the rocket, the modal characteristics of the plate-like structures (such as wings and fins) undergoing accelerated in-plane motions need to be estimated accurately and efficiently.

The modal characteristics of plates were previously studied by many researchers (see, for instance, Ref. [1]). The in-plane motion has also been studied by 3D analysis (see, for instance, Refs. [2–4]). However, study on the modal characteristics of a flexible structure undergoing rigid body motion originates from the famous paper written by Southwell and Gough [5]. Basing on this pioneering study, many researchers provided early analytical grounds on the subject (see, for instance, Refs. [6,7]). Since

*Corresponding author. Tel.: +82 2 2220 0446; fax: +82 2 2293 5070.
E-mail addresses: beyondlimits@hanmail.net (H.S. Lim), hhyoo@hanyang.ac.kr (H.H. Yoo).

0022-460X/$ - see front matter © 2006 Elsevier Ltd. All rights reserved.
doi:10.1016/j.jsv.2006.05.004

1970s, owing to the fast progress of computing technologies, a large number of numerical studies (see, for instance, Refs. [8–10]) followed. In most of the studies, however, flexible structures were idealized as beams. Even if a large number of studies on plate structures exist, only a few of them treat the modal characteristics of plates undergoing rigid body motions. Dokainish and Rawtani [11] employed a finite element method to determine the natural frequencies and the mode shapes of a cantilever plate mounted on a rotating disc. The in-plane stresses are first determined and the increase in the bending stiffness due to the in-plane stresses is obtained to calculate the modal characteristics of the rotating plate. Ramamurti and Kielb [12] extended the previous work to find the modal characteristics of rotating twisted plates. More recently, a linear modeling method employing hybrid deformation variables is proposed by Yoo and Kim [13] to find the modal characteristics of rotating cantilever plates. The Rayleigh–Ritz assumed mode method is employed for the modeling method. Yoo et al. [14] applied the modeling method to find the modal characteristics of rotating composite plates, too. Even if modal characteristics of plates undergoing rotational motions were investigated in the previous studies, those of plates undergoing accelerated in-plane motions have never been studied so far in spite of the practical importance of the subject.

The purpose of the present study is to propose a modeling method by which the modal characteristics (natural frequencies and mode shapes) of plates undergoing accelerated in-plane motions can be estimated accurately. The effects of aspect ratio and dimensionless acceleration on the modal characteristics (natural frequencies and mode shapes) of the accelerated plate will be exhibited and discussed through numerical studies. Some conclusions will be drawn from the numerical results for practical designs of plate-like structures undergoing accelerated in-plane motions.

The accuracy of the proposed modeling method is verified by comparing the numerical results obtained by the proposed modeling method and the finite element method. To obtain the numerical results obtained by the finite element method, the in-plane accelerated motion needs to be replaced by a gravitational field and a nonlinear static analysis should be performed first. The linear modal analysis should be followed to obtain the modal characteristics of the plate. The procedure of employing the finite element method is not as simple as the proposed method. Furthermore, the modeling method proposed in this study employs less degrees of freedom (dof) so that it can be effectively employed for the control of the structure.

2. Formulation for the modal analysis

Fig. 1 shows a cantilever plate that is characterized by length a, width b, and thickness h. The plate is attached to a rigid base A that undergoes accelerated in-plane motion. An orthogonal unit vector triad ($\hat{a}_1, \hat{a}_2,$ and $\hat{a}_3$) that is fixed to the rigid base A constitutes a coordinate system. Point O represents the origin of the coordinate system and point P represents a generic point which lies on the mid-plane of the plate. The mass per unit area, the Poisson's ratio, the Young's modulus, and the shear modulus of the plate are denoted by symbols ρ, ν, E, and G, respectively.

The elastic displacement of the generic point P can be expressed by using the Cartesian deformation variables u_1, u_2, and u_3 as shown in Fig. 2. With the Rayleigh–Ritz assumed mode method being employed, the Cartesian deformation variables u_1, u_2, and u_3 can be approximated as follows:

$$u_1(x,y,t) = \sum_{i=1}^{\mu_1} \phi_{1i}(x,y) q_{1i}(t), \tag{1}$$

$$u_2(x,y,t) = \sum_{i=1}^{\mu_2} \phi_{2i}(x,y) q_{2i}(t), \tag{2}$$

$$u_3(x,y,t) = \sum_{i=1}^{\mu_3} \phi_{3i}(x,y) q_{3i}(t), \tag{3}$$

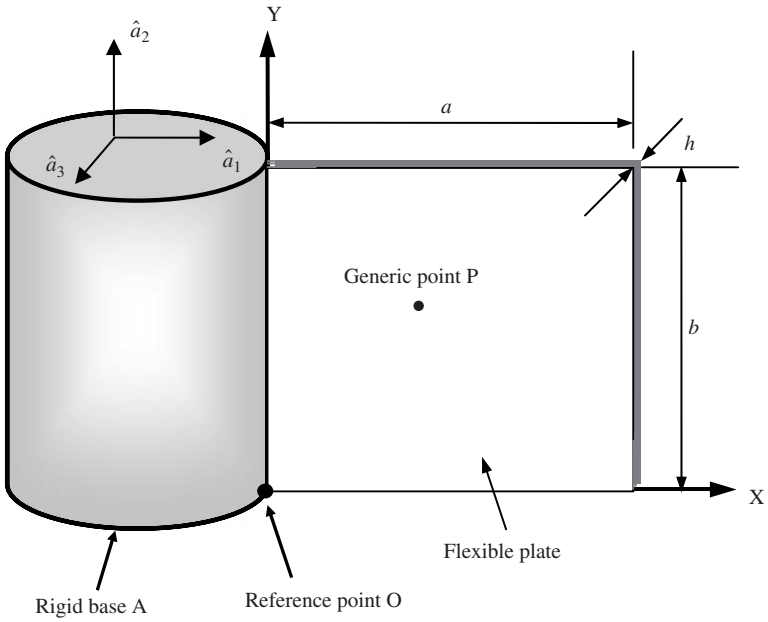

Fig. 1. Configuration of a cantilever plates.

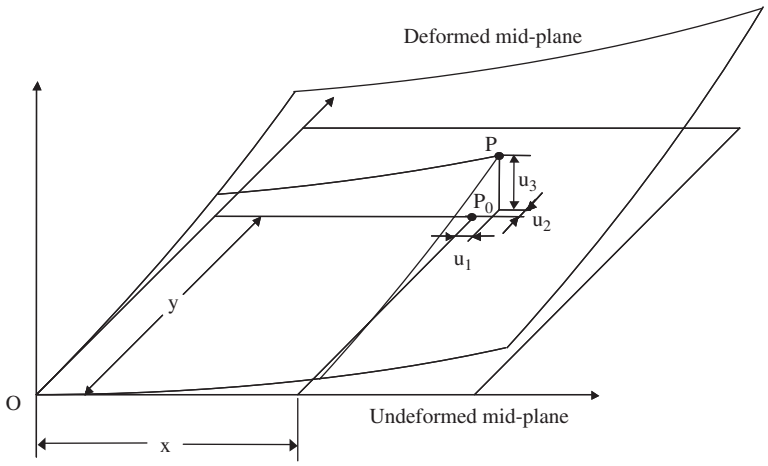

Fig. 2. Deformation variables of a generic point on the mid-plane of a plate.

where μ_1, μ_2, and μ_3 are the numbers of generalized coordinates for the deformation variables u_1, u_2, and u_3, respectively.

To derive the equations of motion for a cantilever plate, the following strain energy expression based on Von Karman strain measures is employed.

$$U = U_b + U_{st} + U_{sh}, \tag{4}$$

where

$$U_b = \frac{1}{2}\int_0^a \int_0^b \frac{Eh^3}{12(1-v^2)}\left[\left(\frac{\partial^2 u_3}{\partial x^2}\right)^2 + \left(\frac{\partial^2 u_3}{\partial y^2}\right)^2 + 2v\left(\frac{\partial^2 u_3}{\partial x^2}\right)\left(\frac{\partial^2 u_3}{\partial y^2}\right) + 2(1-v)\left(\frac{\partial^2 u_3}{\partial x\,\partial y}\right)^2\right] \mathrm{d}y\,\mathrm{d}x, \tag{5}$$

$$U_{st}=\frac{1}{2}\int_0^a\int_0^b\frac{Eh}{(1-\nu^2)}\begin{bmatrix}\left(\frac{\partial u_1}{\partial x}\right)^2+\overline{\varepsilon}_{xx}\left(\frac{\partial u_3}{\partial x}\right)^2+\left(\frac{\partial u_2}{\partial y}\right)^2+\overline{\varepsilon}_{yy}\left(\frac{\partial u_3}{\partial y}\right)^2\\+2\nu\left[\left(\frac{\partial u_1}{\partial x}\right)\left(\frac{\partial u_2}{\partial y}\right)+\frac{1}{2}\overline{\varepsilon}_{xx}\left(\frac{\partial u_3}{\partial y}\right)^2+\frac{1}{2}\overline{\varepsilon}_{yy}\left(\frac{\partial u_3}{\partial x}\right)^2\right]\end{bmatrix}\mathrm{d}y\,\mathrm{d}x, \tag{6}$$

$$U_{sh}=\frac{1}{2}\int_0^a\int_0^b Gh\left[\left(\frac{\partial u_1}{\partial x}\right)^2+2\left(\frac{\partial u_1}{\partial y}\right)\left(\frac{\partial u_2}{\partial x}\right)+\left(\frac{\partial u_1}{\partial x}\right)^2+2\overline{\varepsilon}_{xy}\left(\frac{\partial u_3}{\partial x}\right)\left(\frac{\partial u_3}{\partial y}\right)\right]\mathrm{d}y\,\mathrm{d}x, \tag{7}$$

where U_b, U_{st}, and U_{sh} denote the bending, the stretching, and the in-plane shear strain energies; and $\overline{\varepsilon}_{xx}$, $\overline{\varepsilon}_{yy}$, and $\overline{\varepsilon}_{xy}$ denote the in-plane strains.

With the Kane's method (see Ref. [15]) being employed, the equations of motion can be written as

$$F_i+F_i^*=0\quad(i=1,\ldots,\mu), \tag{8}$$

where μ is the total sum of μ_1, μ_2, and μ_3; and F_i and F_i^* can be obtained with

$$F_i=-\frac{\partial U}{\partial q_i}, \tag{9}$$

$$F_i^*=-\int_0^a\int_0^b\rho\vec{v}_i^P\vec{a}^P\,\mathrm{d}y\,\mathrm{d}x, \tag{10}$$

where q_i consists of q_{1j}, q_{2j}, and q_{3j}; $\vec{v}_i^P$ and $\vec{a}^P$ denote the partial velocity and the acceleration of the point P. The Kirchhoff's assumptions are employed so that the transverse shear and the rotary inertia effects are ignored in this study. The partial velocity of the point P can be easily obtained by differentiating the velocity of P (with respect to $\dot{q}_i$) that can be expressed as follows:

$$\vec{v}^P=(v_x+\dot{u}_1)\hat{a}_1+(v_y+\dot{u}_2)\hat{a}_2+\dot{u}_3\hat{a}_3, \tag{11}$$

where v_x and v_y denote the velocity components of the in-plane motion. Now employing Eqs. (4)–(11), the in-plane equations of motion can be derived as follows:

$$\sum_{j=1}^{\mu_1}\left[\left(\int_0^a\int_0^b\rho\phi_{1i}\phi_{1j}\,\mathrm{d}y\,\mathrm{d}x\right)\ddot{q}_{1j}+\left(\int_0^a\int_0^b\left(\frac{Eh}{(1-\nu^2)}\,\phi_{1i,x}\phi_{1j,x}+Gh\phi_{1i,y}\phi_{1j,y}\right)\mathrm{d}y\,\mathrm{d}x\right)q_{1j}\right]$$
$$+\sum_{j=1}^{\mu_2}\left[\left(\int_0^a\int_0^b\left(\frac{Eh}{(1-\nu^2)}\,\nu\phi_{1i,x}\phi_{2j,y}+Gh\phi_{1i,y}\phi_{2j,x}\right)\mathrm{d}y\,\mathrm{d}x\right)q_{2j}\right]=-\dot{v}_x\left(\int_0^a\int_0^b\rho\phi_{1i}\,\mathrm{d}y\,\mathrm{d}x\right)$$
$$(i=1,2,\ldots,\mu_1), \tag{12}$$

$$\sum_{j=1}^{\mu_2}\left[\left(\int_0^a\int_0^b\rho\phi_{2i}\phi_{2j}\,\mathrm{d}y\,\mathrm{d}x\right)\ddot{q}_{2j}+\left(\int_0^a\int_0^b\left(\frac{Eh}{(1-\nu^2)}\,\phi_{2i,y}\phi_{2j,y}+Gh\phi_{2i,x}\phi_{2j,x}\right)\mathrm{d}y\,\mathrm{d}x\right)q_{2j}\right]$$
$$+\sum_{j=1}^{\mu_1}\left[\left(\int_0^a\int_0^b\left(\frac{Eh}{(1-\nu^2)}\,\nu\phi_{2i,x}\phi_{1j,y}+Gh\phi_{2i,y}\phi_{1j,x}\right)\mathrm{d}y\,\mathrm{d}x\right)q_{1j}\right]=-\dot{v}_y\left(\int_0^a\int_0^b\rho\phi_{2i}\,\mathrm{d}y\,\mathrm{d}x\right)$$
$$(i=1,2,\ldots,\mu_2), \tag{13}$$

where a subscript following a comma indicates the partial differentiation with respect to the subscript. For instance, $\phi_{i,y}$ denotes the partial derivative of ϕ_i with respect to y. If $\dot{v}_x$ and $\dot{v}_y$ are constant, the steady-state solutions for q_{1i} and q_{2i} (denoted as $\overline{q}_{1i}$ and $\overline{q}_{2i}$ hereinafter) can be obtained from Eqs. (12) and (13).

After obtaining the steady-state solutions $\overline{q}_{1i}$ and $\overline{q}_{2i}$, one can derive the constant in-plane strain measures $\overline{\varepsilon}_{xx}$, $\overline{\varepsilon}_{yy}$, and $\overline{\varepsilon}_{xy}$ as follows:

$$\begin{aligned}
\overline{\varepsilon}_{xx} &= \left(\frac{\partial u_1}{\partial x}\right) = \sum_{i=1}^{\mu_1} \phi_{1i,x}\overline{q}_{1i},\\
\overline{\varepsilon}_{yy} &= \left(\frac{\partial u_2}{\partial y}\right) = \sum_{i=1}^{\mu_2} \phi_{2i,y}\overline{q}_{2i},\\
\overline{\varepsilon}_{xy} &= \left(\frac{\partial u_1}{\partial y}\right) + \left(\frac{\partial u_2}{\partial x}\right) = \sum_{i=1}^{\mu_1} \phi_{1i,y}\overline{q}_{1i} + \sum_{i=1}^{\mu_2} \phi_{2i,x}\overline{q}_{2i}.
\end{aligned} \tag{14}$$

Substituting Eq. (14) into the bending strain energy, the linear bending equations can be derived as follows:

$$\sum_{j=1}^{\mu_3}\left[\begin{array}{c}
\left(\int_0^a\int_0^b \rho\phi_{3i}\phi_{3j}\,\mathrm{d}y\,\mathrm{d}x\right)\ddot{q}_{3j}\\
+\left(\int_0^a\int_0^b \frac{Eh^3}{12(1-\nu^2)}\left(\begin{array}{c}\phi_{3i,xx}\phi_{3j,xx}+\phi_{3i,yy}\phi_{3j,yy}+\nu\phi_{3i,xx}\phi_{3j,yy}\\ +\nu\phi_{3i,yy}\phi_{3j,xx}+2(1-\nu)\phi_{3i,xy}\phi_{3j,xy}\end{array}\right)\mathrm{d}y\,\mathrm{d}x\right)q_{3j}\\
+\left(\int_0^a\int_0^b \frac{Eh}{(1-\nu^2)}\left(\begin{array}{c}\overline{\varepsilon}_{xx}(\phi_{3i,x}\phi_{3j,y}+\nu\phi_{3i,y}\phi_{3j,y})\\ +\overline{\varepsilon}_{yy}(\phi_{3i,y}\phi_{3j,y}+\nu\phi_{3i,x}\phi_{3j,x})\end{array}\right)\mathrm{d}y\,\mathrm{d}x\right)q_{3j}\\
+\left(\int_0^a\int_0^b G h\overline{\varepsilon}_{xy}(\phi_{3i,y}\phi_{3j,x}+\phi_{3i,x}\phi_{3j,y})\mathrm{d}y\,\mathrm{d}x\right)q_{3j}
\end{array}\right] = 0$$
$$(i=1,2,\ldots,\mu_3). \tag{15}$$

As shown in the third and the fourth lines in Eq. (15), extra bending stiffness terms appear due to the in-plane strains induced by the accelerated in-plane motion. Therefore, as the acceleration varies, these terms play important roles for the modal analysis of cantilever plates undergoing accelerated in-plane motion.

In order to rewrite Eq. (15) in a dimensionless form, the following dimensionless variables and parameters are introduced.

$$\begin{gathered}
\tau \equiv \tfrac{t}{T}, \quad \xi \equiv \tfrac{x}{a}, \quad \eta \equiv \tfrac{y}{a},\\
\delta \equiv \tfrac{a}{b}, \quad \sigma \equiv \tfrac{a}{h}, \quad \beta = \tfrac{G(1-\nu^2)}{E},\\
\vartheta_{aj} \equiv \tfrac{q_{aj}}{a}, \quad \phi_{ai}(x,y) \equiv \varphi_{ai}(\xi,\eta),
\end{gathered} \tag{16}$$

where T is defined as

$$T \equiv \sqrt{\frac{12(1-\nu^2)\rho a^4}{Eh^3}}. \tag{17}$$

Using the dimensionless variables and parameters, a dimensionless form of Eq. (15) can be obtained as follows:

$$\sum_{j=1}^{\mu_3}\left[\begin{array}{c}
\left(\int_0^1\int_0^1 \varphi_{3i}\varphi_{3j}\,\mathrm{d}\eta\,\mathrm{d}\xi\right)\ddot{\vartheta}_{3j}\\
+\left(\int_0^1\int_0^1 \left(\begin{array}{c}\delta^4\varphi_{3i,\eta\eta}\,\varphi_{3j,\eta\eta}+2\nu\delta^2\varphi_{3i,\xi\xi}\,\varphi_{3j,\eta\eta}\\ +\varphi_{3i,\xi\xi}\,\varphi_{3j,\xi\xi}+2(1-\nu)\delta^2\varphi_{3i,\xi\eta}\,\varphi_{3j,\xi\eta}\end{array}\right)\mathrm{d}\eta\,\mathrm{d}\xi\right)\vartheta_{3j}\\
+\left(\int_0^1\int_0^1 12\sigma^2\left(\begin{array}{c}\overline{\varepsilon}_{xx}(\varphi_{3i,\xi}\,\varphi_{3j,\xi}+\delta^2\nu\varphi_{3i,\eta}\,\varphi_{3j,\eta})\\ +\overline{\varepsilon}_{yy}(\delta^2\varphi_{3i,\eta}\,\varphi_{3j,\eta}+\nu\varphi_{3i,\xi}\,\varphi_{3j,\xi})\end{array}\right)\mathrm{d}\eta\,\mathrm{d}\xi\right)\vartheta_{3j}\\
+\left(\int_0^1\int_0^1 12\sigma^2\delta\beta\overline{\varepsilon}_{xy}(\varphi_{3i,\eta}\,\varphi_{3j,\xi}+\varphi_{3i,\xi}\,\varphi_{3j,\eta})\mathrm{d}\eta\,\mathrm{d}\xi\right)\vartheta_{3j}
\end{array}\right] = 0.$$
$$(i=1,2,\ldots,\mu_3). \tag{18}$$

The in-plane dimensionless static equations (which provide the dimensionless particular solutions of the differential equations, Eqs. (12) and Eq. (13)) can be written as follows:

$$\sigma^2\sum_{j=1}^{\mu_1}\left[\left(\int_0^1\int_0^1(12\varphi_{1i,\xi}\,\varphi_{1j,\xi}+12\delta^2\beta\varphi_{1i,\eta}\,\varphi_{1j,\eta})\mathrm{d}\eta\,\mathrm{d}\xi\right)\vartheta_{1j}\right]$$
$$+\sigma^2\sum_{j=1}^{\mu_2}\left[\left(\int_0^1\int_0^1(12\delta\varphi_{1i,\xi}\,\varphi_{2j,\eta}+12\delta\beta\varphi_{1i,\eta}\,\varphi_{2j,\xi})\mathrm{d}\eta\,\mathrm{d}\xi\right)\vartheta_{2j}\right]$$
$$=-\alpha_x\left(\int_0^1\int_0^1\varphi_{1i}\,\mathrm{d}\eta\,\mathrm{d}\xi\right)\quad(i=1,2,\ldots,\mu_1),\tag{19}$$

$$\sigma^2\sum_{j=1}^{\mu_2}\left[\left(\int_0^1\int_0^1(12\delta^2\varphi_{2i,\eta}\,\varphi_{2j,\eta}+12\beta\varphi_{2i,\xi}\,\varphi_{2j,\xi})\mathrm{d}\eta\,\mathrm{d}\xi\right)\vartheta_{2j}\right]$$
$$+\sigma^2\sum_{j=1}^{\mu_1}\left[\left(\int_0^1\int_0^1(12\delta\varphi_{2i,\xi}\,\varphi_{1j,\eta}+12\delta\beta\varphi_{2i,\eta}\,\varphi_{1j,\xi})\mathrm{d}\eta\,\mathrm{d}\xi\right)\vartheta_{1j}\right]$$
$$=-\alpha_y\left(\frac{1}{\delta}\int_0^1\int_0^1\varphi_{2i}\,\mathrm{d}\eta\,\mathrm{d}\xi\right)\quad(i=1,2,\ldots,\mu_2).\tag{20}$$

In the above equations

$$\alpha_x\equiv\frac{\dot{v}_x}{A_x},\quad \alpha_y\equiv\frac{\dot{v}_y}{A_y},\tag{21}$$

where

$$A_x=\frac{a}{T^2},\quad A_y=\frac{b}{T^2}.\tag{22}$$

One can easily see that $\sigma^2\vartheta_{ai}$ which can be obtained from Eqs. (19) and (20) is independent of σ. Since the in-plane strain measures can be now obtained as

$$\overline{\varepsilon}_{xx}=\sum_{i=1}^{\mu_1}\phi_{1i,x}\overline{q}_{1i}=\sum_{i=1}^{\mu_1}\varphi_{1i,\xi}\overline{\vartheta}_{1i},$$
$$\overline{\varepsilon}_{yy}=\sum_{i=1}^{\mu_2}\phi_{2i,y}\overline{q}_{2i}=\sum_{i=1}^{\mu_2}\varphi_{2i,\eta}\overline{\vartheta}_{2i},$$
$$\overline{\varepsilon}_{xy}=\sum_{i=1}^{\mu_1}\phi_{1i,y}\overline{q}_{1i}+\sum_{i=1}^{\mu_2}\phi_{2i,x}\overline{q}_{2i}=\sum_{i=1}^{\mu_1}\varphi_{1i,\eta}\vartheta_{1i}+\sum_{i=1}^{\mu_2}\varphi_{2i,\xi}\vartheta_{2i}.\tag{23}$$

$\sigma^2\overline{\varepsilon}_{xx}$, $\sigma^2\overline{\varepsilon}_{yy}$, and $\sigma^2\overline{\varepsilon}_{xy}$ are independent of σ. Let's introduce $\tilde{\varepsilon}_{xx}$, $\tilde{\varepsilon}_{yy}$, and $\tilde{\varepsilon}_{xy}$ as follows:

$$\tilde{\varepsilon}_{xx}=\sigma^2\overline{\varepsilon}_{xx},$$
$$\tilde{\varepsilon}_{yy}=\sigma^2\overline{\varepsilon}_{yy},$$
$$\tilde{\varepsilon}_{xy}=\sigma^2\overline{\varepsilon}_{xy}.\tag{24}$$

Then Eq. (18) can be rewritten as follows:

$$\sum_{j=1}^{\mu_3}\left[\begin{array}{c}\left(\int_0^1\int_0^1 \varphi_{3i}\varphi_{3j}\,\mathrm{d}\eta\,\mathrm{d}\xi\right)\ddot{\vartheta}_{3j}\\ +\left(\int_0^1\int_0^1\left(\begin{array}{c}\delta^4\varphi_{3i,\eta\eta}\,\varphi_{3j,\eta\eta}+2\nu\delta^2\varphi_{3i,\xi\xi}\,\varphi_{3j,\eta\eta}\\ +\varphi_{3i,\xi\xi}\,\varphi_{3j,\xi\xi}+2(1-\nu)\delta^2\varphi_{3i,\xi\eta}\,\varphi_{3j,\xi\eta}\end{array}\right)\mathrm{d}\eta\,\mathrm{d}\xi\right)\vartheta_{3j}\\ +\left(\int_0^1\int_0^1 12\left(\begin{array}{c}\tilde{\varepsilon}_{xx}(\varphi_{3i,\xi}\,\varphi_{3j,\xi}+\delta^2\nu\varphi_{3i,\eta}\,\varphi_{3j,\eta})\\ +\tilde{\varepsilon}_{yy}(\delta^2\varphi_{3i,\eta}\,\varphi_{3j,\eta}+\nu\varphi_{3i,\xi}\,\varphi_{3j,\xi})\end{array}\right)\mathrm{d}\eta\,\mathrm{d}\xi\right)\vartheta_{3j}\\ +\left(\int_0^1\int_0^1 12\delta\beta\tilde{\varepsilon}_{xy}(\varphi_{3i,\eta}\,\varphi_{3j,\xi}+\varphi_{3i,\xi}\,\varphi_{3j,\eta})\mathrm{d}\eta\,\mathrm{d}\xi\right)\vartheta_{3j}\end{array}\right]=0. \tag{25}$$

Table 1
Lowest five dimensionless natural frequencies obtained by the present method and a commercial finite element code with $\nu = 0.2$, $\beta = 0.4$, $\delta = 1$, $\alpha_x = 0$

Acceleration	Method	Dimensionless natural frequencies				
		1st	2nd	3rd	4th	5th
$\alpha_y = 0$	Present	3.5040	8.9438	21.768	27.660	32.113
	ANSYS	3.4929	8.9291	21.727	27.559	32.064
$\alpha_y = 5$	Present	3.4752	8.8908	21.742	27.622	32.144
	ANSYS	3.4622	8.8773	21.697	27.516	32.082
$\alpha_y = 10$	Present	3.3835	8.7319	21.661	27.513	32.233
	ANSYS	3.3759	8.7170	21.629	27.393	32.167

Table 2
Lowest five dimensionless natural frequencies obtained by the present method and a commercial finite element code with $\nu = 0.3$, $\beta = 0.35$, $\delta = 1$, $\alpha_x = 0$

Acceleration	Method	Dimensionless natural frequencies				
		1st	2nd	3rd	4th	5th
$\alpha_y = 0$	Present	3.4767	8.5235	21.345	27.279	31.047
	ANSYS	3.4720	8.5312	21.334	27.219	31.074
$\alpha_y = 5$	Present	3.4464	8.4618	21.264	27.214	31.046
	ANSYS	3.4399	8.4542	21.248	27.159	31.074
$\alpha_y = 10$	Present	3.3365	8.3089	21.146	27.136	31.134
	ANSYS	3.3393	8.2926	21.126	27.092	31.187

Table 3
Lowest five dimensionless natural frequencies obtained by the present method and a commercial finite element code with $\nu = 0.3$, $\beta = 0.35$, $\delta = 2$, $\alpha_x = 0$

Acceleration	Method	Dimensionless natural frequencies				
		1st	2nd	3rd	4th	5th
$\alpha_y = 0$	Present	3.4511	14.836	21.560	48.388	60.397
	ANSYS	3.4406	14.824	21.452	48.314	60.242
$\alpha_y = 5$	Present	3.4361	14.776	21.592	48.339	60.463
	ANSYS	3.4294	14.771	21.498	48.276	60.383
$\alpha_y = 10$	Present	3.3895	14.601	21.683	48.193	60.559
	ANSYS	3.3821	14.593	21.597	48.123	60.482

As can be observed from Eq. (25), the dimensionless modal characteristics of the cantilever plate undergoing accelerated in-plane motion are related to the parameters of β and δ. It can be also observed from Eqs. (19) and (20) that the modal characteristics are affected by the dimensionless acceleration components α_x and α_y. The parameter σ, however, does not affect the dimensionless modal characteristics of the accelerated plate since $\tilde{\varepsilon}_{ab}$'s are independent of σ.

In the following section, Eq. (25) along with Eqs. (19)–(24) will be employed for the modal analysis of cantilever plates undergoing accelerated in-plane motion. The effects of dimensionless acceleration components α_x and α_y along with the dimensionless parameters β and δ on the modal characteristics of the accelerated plate will be investigated.

3. Numerical results

In this section, modal analysis results are obtained by employing the equations derived in the previous section. The assumed mode functions for a cantilever plate are constructed by using cantilever beam functions

Table 4
Lowest five dimensionless natural frequencies obtained by the present method and a commercial finite element code with $\nu = 0.3$, $\beta = 0.35$, $\delta = 1$, $\alpha_y = 0$

Acceleration	Method	Dimensionless natural frequencies				
		1st	2nd	3rd	4th	5th
$\alpha_x = 0$	Present	3.4767	8.5235	21.345	27.279	31.047
	ANSYS	3.4720	8.5312	21.334	27.219	31.074
$\alpha_x = 3$	Present	2.7236	8.2433	20.805	27.137	30.629
	ANSYS	2.7201	8.2509	20.797	27.093	30.650
$\alpha_x = 6$	Present	1.6427	7.9491	20.196	27.014	30.217
	ANSYS	1.6392	7.9539	20.190	26.979	30.247

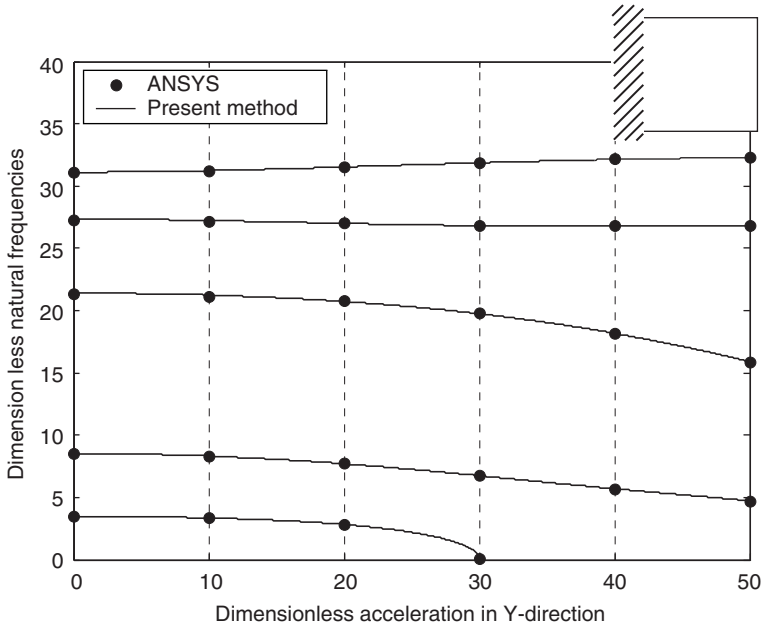

Fig. 3. Variations of the lowest five dimensionless natural frequencies versus dimensionless acceleration α_y ($\delta = 1.0$, $\beta = 0.35$, $\nu = 0.3$, $\alpha_x = 0$).

and free-free beam functions. The beam mode functions are generated in polynomial forms by using the Gram-Schmidt method. The detailed procedure to generate the mode functions is given in Refs. [16–18]. In the present study, 5 cantilever beam functions and 7 free-free beam functions (including 2 rigid body mode functions) are employed to generate 35 mode functions for the cantilever plate.

To verify the accuracy of the modal analysis results obtained by the present method, a commercial finite element code (see Ref. [19]) was employed. Since it is not possible to prescribe an accelerated motion with the commercial finite element code, a stationary plate undertaking a gravitational force is analyzed instead. To create the same inertia force effect induced by an accelerated motion, an equivalent gravitational field is applied to the stationary plate. By applying the artificial gravitational field to the plate, in-plane strains were first obtained by using the nonlinear static analysis module of the commercial code. Then the modal characteristics of the plate (with the in-plane strains) were calculated by using the modal analysis module of the commercial code. With the commercial code, a finite element model having one hundred identical shell63 elements (number of nodes is 121 and the degree of freedom is 726) is employed. On the other hand, only 35 dof are employed for the present modeling method.

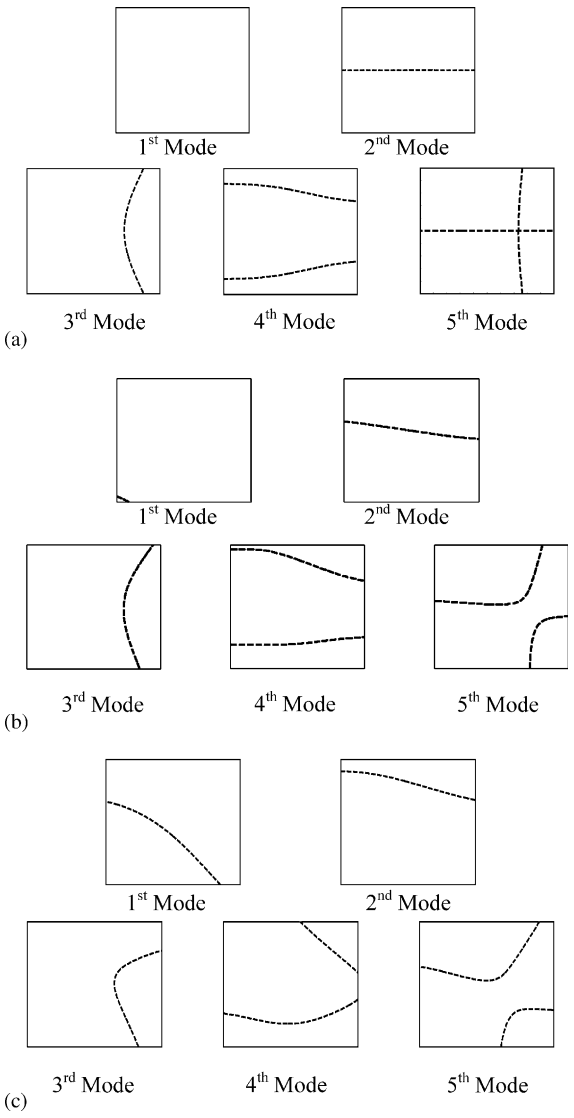

Fig. 4. Nodal line patterns of lowest five mode shapes with different accelerations α_y ($\delta = 1.0$, $\beta = 0.35$, $v = 0.3$, $\alpha_x = 0$).

Tables 1–4 show the lowest five dimensionless natural frequencies obtained by the present method and a commercial finite element program. Different combinations of β, δ, α_x, and α_y are employed for the tables. The effects of the dimensionless acceleration (α_x or α_y) and parameters on the lowest five natural frequencies are shown in the tables. As can be observed, the results obtained by the present method are in good agreement

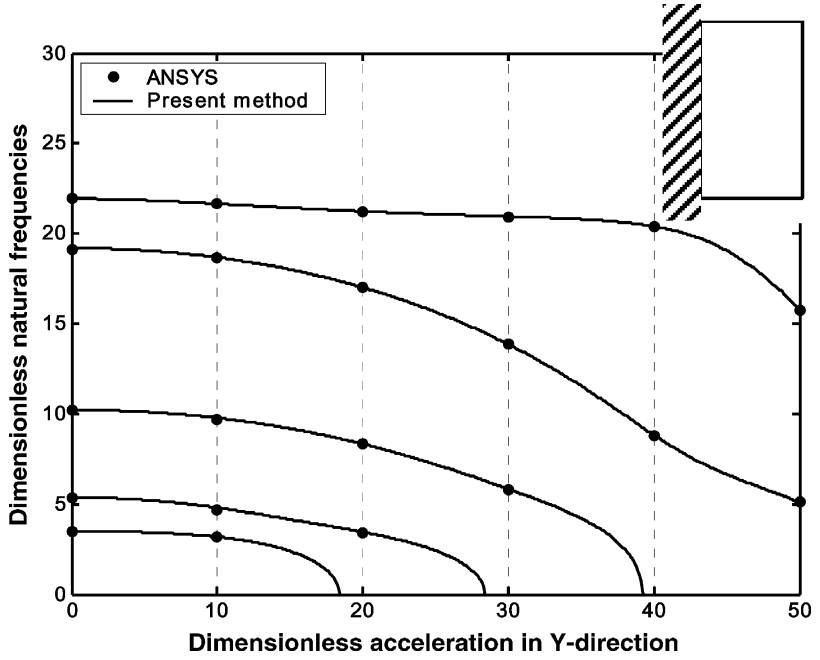

Fig. 5. Variations of the lowest five dimensionless natural frequencies versus dimensionless acceleration α_y ($\delta = 0.5$, $\beta = 0.35$, $v = 0.3$, $\alpha_x = 0$).

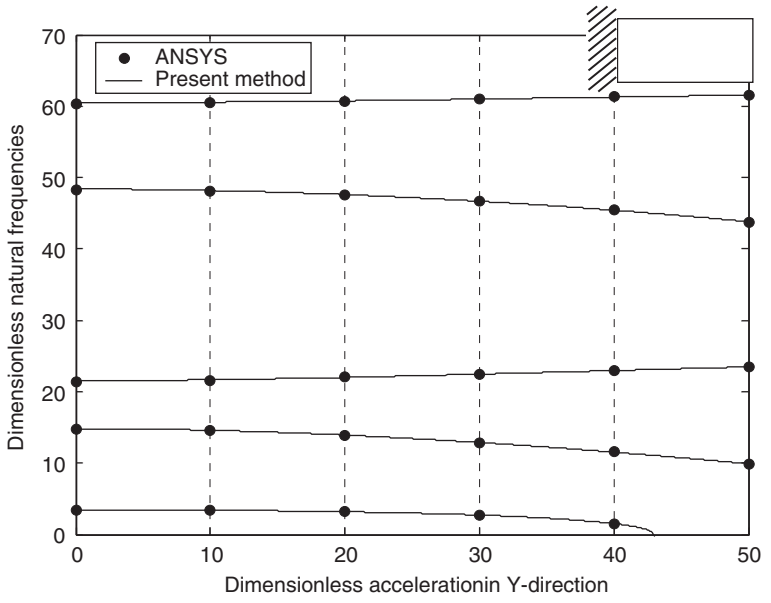

Fig. 6. Variations of the lowest five dimensionless natural frequencies versus dimensionless acceleration α_y ($\delta = 2.0$, $\beta = 0.35$, $v = 0.3$, $\alpha_x = 0$).

with those obtained by the commercial code (the discrepancy between the two results is always less than 0.5%).

Fig. 3 shows the variations of the lowest five dimensionless natural frequencies versus the dimensionless acceleration α_y (when the dimensionless acceleration α_x is equal to 0). The results obtained by the present method are in good agreement with those obtained with the commercial finite element code. The parameters employed for the analysis are as follows: $\delta = 1$, $\nu = 0.3$, and $\beta = 0.35$. As shown in the figure, the lowest three natural frequencies decrease as the dimensionless acceleration α_y increases. Especially, the first natural frequency becomes zero when the dimensionless acceleration α_y is equal to 30. In other words, dynamic buckling occurs if the dimensionless acceleration exceeds the value.

Fig. 4 shows the variations of the lowest five mode shapes of the plate. The dotted lines represent the nodal lines of the mode shapes. The five modes (when $\alpha_y = 0$) represent the first bending mode, the torsional mode, the second bending mode, the chord-wise bending mode, and the combination mode, respectively. As shown in the figures, when the cantilever plate is accelerated in Y-direction, all the symmetries of the nodal lines are destroyed. The nodal line of the first mode (when $\alpha_y = 30$) provides useful information about the dynamic buckling mode of the accelerated plate.

Figs. 5 and 6 show the variations of the lowest five dimensionless natural frequencies versus the dimensionless acceleration α_y with aspect ratios $\delta = 0.5$ and 2, respectively. All the other parameter values employed to obtain the results are same as those to obtain the results of Fig. 3. The first natural frequency with the aspect ratio $\delta = 0.5$ decreases faster (comparing to the case of $\delta = 1$) as the acceleration increases and the dynamic buckling occurs faster, too. On the other hand, with the aspect ratio $\delta = 2$, the first natural frequency decreases slower and dynamic buckling occurs with a larger acceleration. Particularly note that the third natural frequency (the second bending mode) increases rather than decreases in this case as the acceleration increases.

Fig. 7 shows the variations of the lowest five dimensionless natural frequencies versus the dimensionless acceleration α_y with $\delta = 1$, $\nu = 0.2$, and $\beta = 0.4$. All the other parameter values employed to obtain the results are same as those to obtain the results of Fig. 3. As can be observed from this figure, the modal characteristics of the plate change slightly. Dynamic buckling occurs with acceleration slightly larger than that shown in Fig. 3.

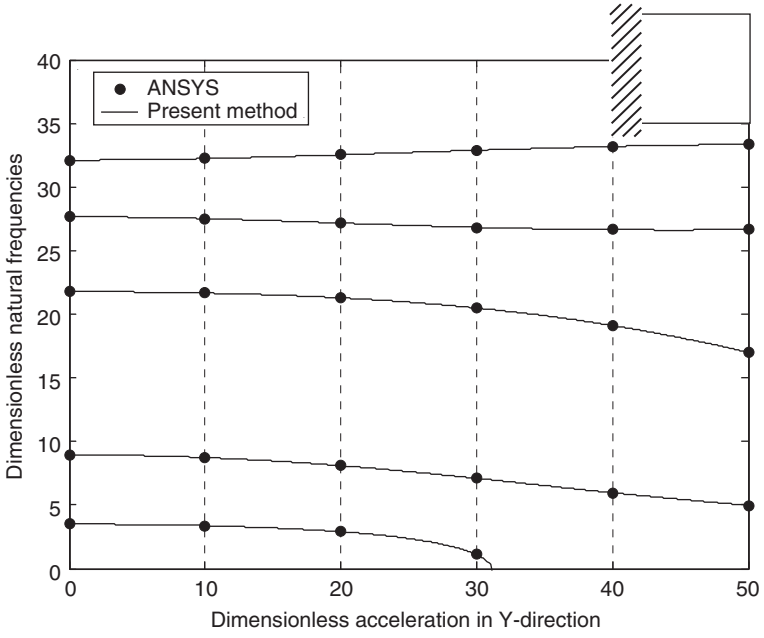

Fig. 7. Variations of the lowest five dimensionless natural frequencies versus dimensionless acceleration α_y ($\delta = 1.0$, $\beta = 0.4$, $\nu = 0.2$, $\alpha_x = 0$).

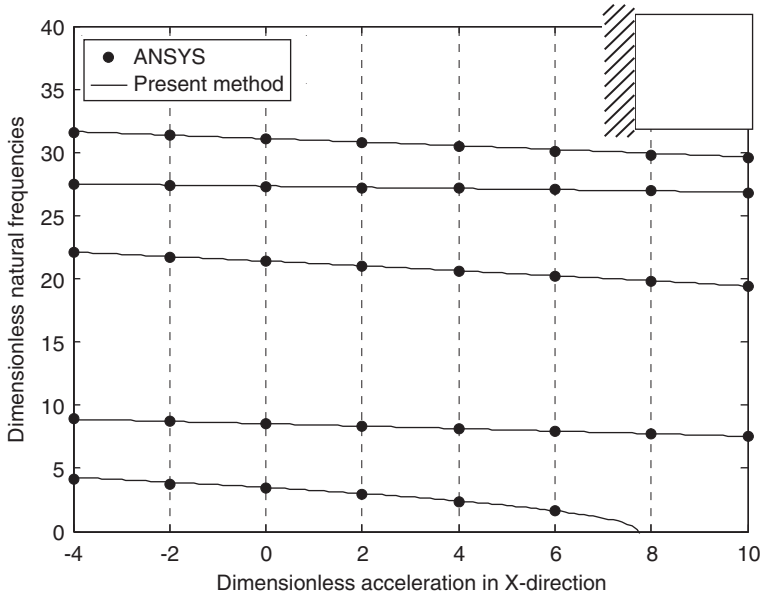

Fig. 8. Variations of the lowest five dimensionless natural frequencies versus dimensionless acceleration α_x ($\delta = 1.0$, $\beta = 0.35$, $v = 0.3$, $\alpha_y = 0$).

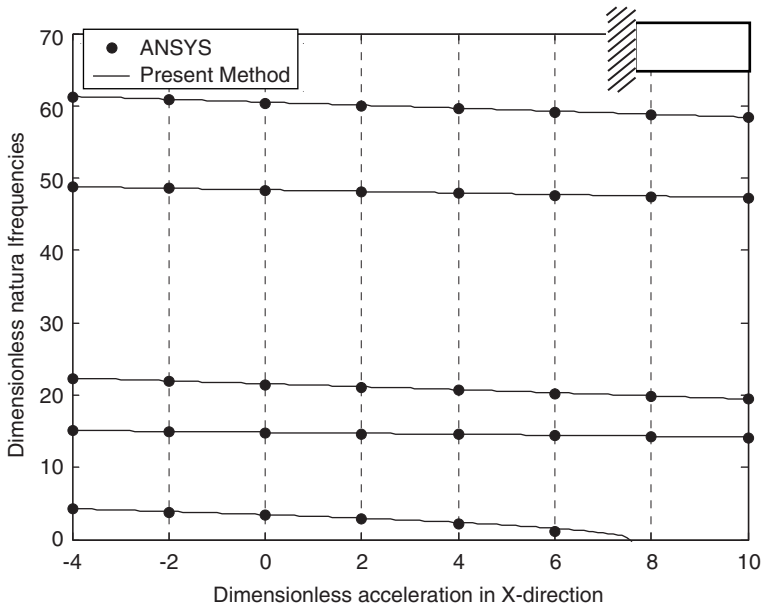

Fig. 9. Variations of the lowest five dimensionless natural frequencies versus dimensionless acceleration α_x ($\delta = 2.0$, $\beta = 0.35$, $v = 0.3$, $\alpha_y = 0$).

Figs. 8–10 show the variations of the lowest five dimensionless natural frequencies versus the dimensionless acceleration α_x with aspect ratios $\delta = 1$, 2, and 0.5. All the other parameter values employed to obtain the results are same as those to obtain the results of Fig. 3. As shown in these figures, all the natural frequencies decrease as the acceleration increases. Note also that the value of dynamic buckling acceleration decreases slightly as the aspect ratio increases.

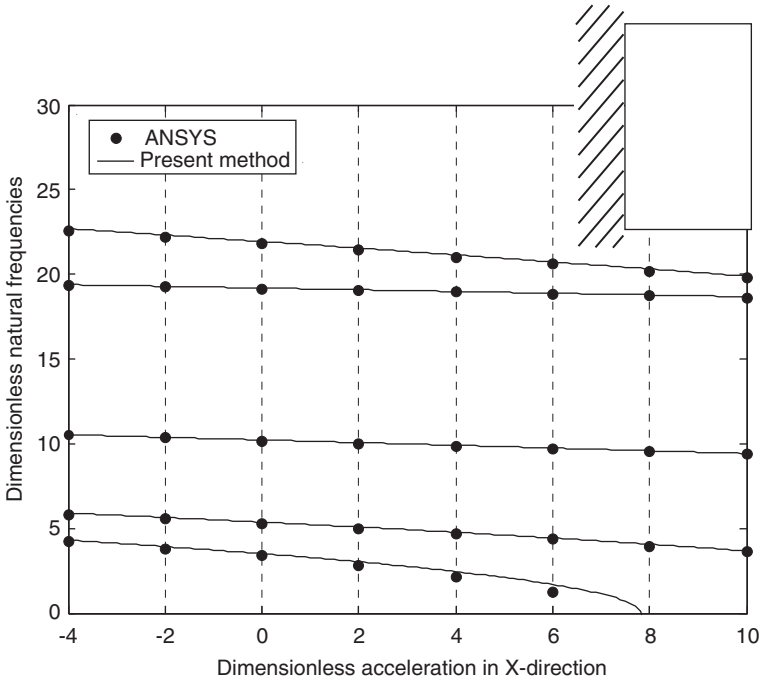

Fig. 10. Variations of the lowest five dimensionless natural frequencies versus dimensionless acceleration α_x ($\delta = 0.5$, $\beta = 0.35$, $v = 0.3$, $\alpha_x = 0$).

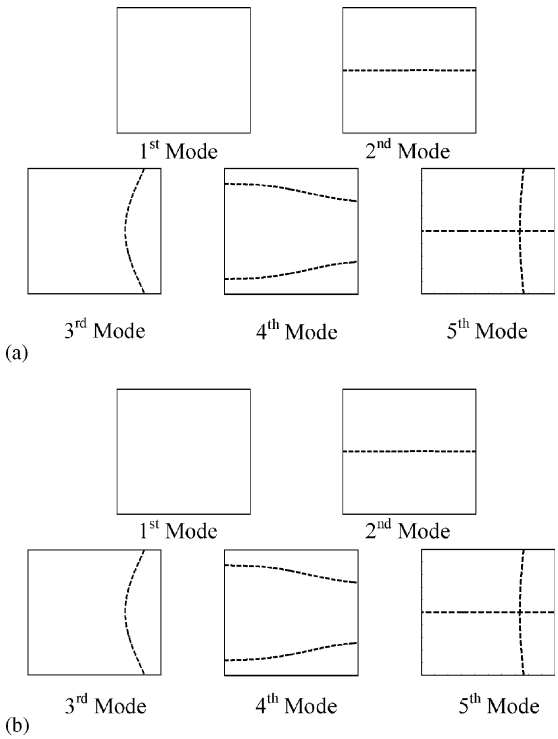

Fig. 11. Nodal line patterns of lowest five mode shapes with different accelerations α_x ($\delta = 1.0$, $\beta = 0.35$, $v = 0.3$, $\alpha_y = 0$).

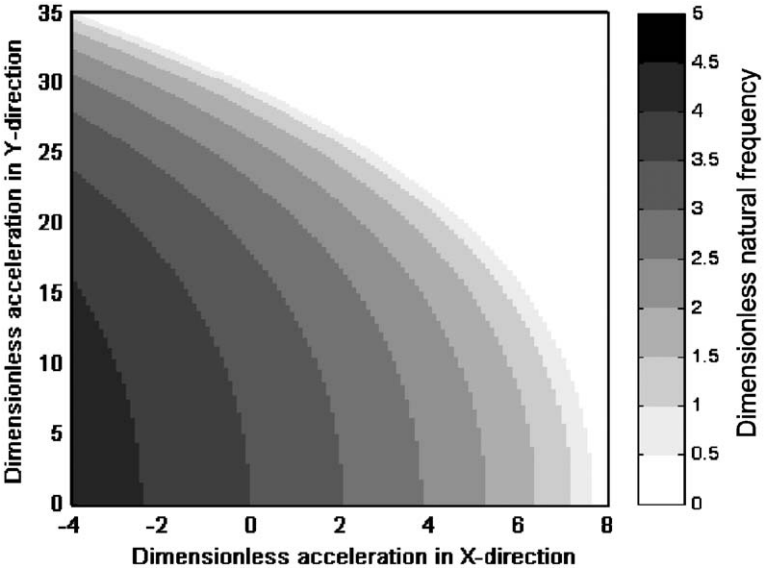

Fig. 12. Variations of the first dimensionless natural frequency versus dimensionless acceleration components α_x and α_y ($\delta = 1.0$, $\beta = 0.35$, $\nu = 0.3$).

Fig. 11 shows the variations of the lowest five mode shapes of the plate that is accelerated in X-direction. The dotted lines represent the nodal lines of the mode shapes. As shown in the figures, when the cantilever plate is accelerated in X-direction, all the symmetries of the nodal lines are preserved. Different from the case of being accelerated in Y-direction, the mode shapes do not change significantly.

Fig. 12 shows the variations of the first dimensionless natural frequency versus the dimensionless accelerations α_x and α_y. All the other parameter values employed to obtain the results are same as those to obtain the results of Fig. 3. As show in this figure, the natural frequency is more affected by the acceleration component in X-direction than that in Y-direction.

4. Conclusion

In this study, dimensionless equations for the modal analysis of a rectangular plate undergoing accelerated in-plane motion are derived. Employing the equations, it is shown that two dimensionless in-plane acceleration components as well as the aspect ratio influence the dimensionless modal characteristics of the plate significantly. Due to the in-plane strain induced by the accelerated motion, natural frequencies of the plate usually decrease as the acceleration increases. It is exhibited that dynamic buckling (when the first natural frequency becomes null) occurs when the acceleration components exceed some critical values. As the aspect ratio decreases, the critical value for the acceleration component in Y-direction decreases significantly while that in X-direction increases slightly. Incidentally, when the plate is accelerated in X-direction, the nodal lines of mode shapes do not change significantly and preserve their symmetry. However, when it is accelerated in Y-direction, they change significantly and loose the symmetry. In general, the X-direction acceleration component affects the natural frequency variation more than the Y-direction acceleration component does. Lastly, it is shown that the plate thickness ratio does not influence the dimensionless modal characteristics while Poisson's ratio does slightly.

Acknowledgments

This research was supported by Center of Innovative Design Optimization Technology (iDOT), Korea Science and Engineering Foundation.

References

[1] K.M. Liew, Y. Xiang, S. Kitipornchai, Research on thick plate vibration: A literature survey, *Journal of Sound and Vibration* 180 (1995) 163–176.
[2] K.M. Liew, K.C. Hung, M.K. Lim, A continuum three-dimensional vibration analysis of thick rectangular plates, *International Journal of Solids and Structures* 30 (1993) 3357–3379.
[3] K.M. Liew, K.C. Hung, M.K. Lim, Three-dimensional elasticity solutions to vibration of cantilevered skewed trapezoids, *AIAA Journal* 32 (1994) 2080–2089.
[4] K.M. Liew, K.C. Hung, M.K. Lim, Three-dimensional vibration of rectangular plates: Variance of simple support conditions and influence of in-plane inertia, *International Journal of Solids and Structures* 31 (1994) 3233–3247.
[5] R. Southwell, F. Gough, The free transverse vibration of airscrew blades, British A. R. C. Reports and Memoranda, No. 766, 1921.
[6] T. Theodorsen, Propeller Vibrations and the Effect of Centrifugal Force, NASA TN, No. 516. 1935.
[7] M. Schilhansl, Bending frequency of a rotating cantilever beam, *Transaction of ASME, Journal of Applied Mechanics* 25 (1958) 28–30.
[8] S. Putter, H. Manor, Natural frequencies of radial rotating beams, *Journal of Sound and Vibration* 56 (1978) 175–185.
[9] R. Bhat, Transverse vibration of a rotating uniform cantilever beam with tip mass as predicted by using beam characteristic orthogonal polynomials in the Rayleigh–Ritz Method, *Journal of Sound and Vibration* 105 (1986) 199–210.
[10] K.M. Liew, M.K. Lim, Transverse vibration of trapezoidal plates of variable thickness: symmetric trapezoidals, *Journal of Sound and Vibration* 165 (1993) 45–67.
[11] M. Dokainish, S. Rawtani, Vibration analysis of rotating cantilever plates, *International Journal for Numerical Methods in Engineering* 3 (1971) 233–248.
[12] V. Ramamurti, R. Kielb, Natural frequencies of twisted rotating plates, *Journal of Sound and Vibration* 97 (1984) 429–449.
[13] H. Yoo, S. Kim, Free vibration analysis of rotating cantilever plates, *AIAA Journal* 40 (2002) 2188–2196.
[14] H. Yoo, S. Kim, D. Inman, Modal analysis of rotating composite cantilever plates, *Journal of Sound and Vibration* 258 (2002) 233–246.
[15] T. Kane, D. Levinson, *Dynamics: Theory and Applications*, McGraw-Hill, New York, 1985.
[16] T. Chihara, *An Introduction to Orthogonal Polynomials*, Gordon and Breach Science Publishers, London, 1978.
[17] R. Bhat, Natural frequencies of rectangular plates using characteristic orthogonal polynomials in Rayleigh–Ritz Method, *Journal of Sound and Vibration* 102 (1985) 493–499.
[18] A.W. Leissa, Vibration of Plates, *NASA SP* 160 (1969).
[19] ANSYS, *User's Manual, Structural Analysis Guide*, ANSYS Inc, 1998.